Chapter 2

Design Concepts of Single-Tooth Winding DSSRM

2.1 Introduction

The development of double-stator SRMs (DSSRMs) drastically improved the torque and power density of SRMs. The single-tooth winding add-on further enhances its compactness and high-efficiency speed range making it a strong substitute for PM motors [55, 56]. The geometric and magnetic configuration of a single-tooth winding DSSRM accomplish the following advantages:

1. Higher output torque because of the better utilisation of machine volume by the introduction of segmented rotor and second stator.

2. Compact and higher fault-tolerant windings because of the non-overlapping structure.

3. Reduce unaligned inductance because of the cancellation of the inner and outer stator fluxes near unaligned position.

4. Lower acoustic noise and vibration because of the reduced normal component of air-gap flux density.

In this chapter, the design procedure for single-tooth winding DSSRM has been discussed together with the investigation of some further improvements. The torque equation of the machine is derived. The calculation of the arc angles of the stator/rotor

poles for maximum aligned and minimum unaligned inductance is discussed. The selection criteria for slot/segment combination and winding polarity are illustrated.

2.2 Single-tooth winding DSSRM

2.2.1 The topology

In the radial flux single-tooth winding DSSRM, a segmented rotor is placed between two stators; inner and outer, and shares the magnetic fluxes of both. Fig. 2.1 illustrates the structure of a 3-phase 12/10/12 pole motor of such configuration. Fig. 2.1 (a) represents its 2-D cross-sectional view with only phase A windings shown. The windings of phase B and phase C will be -60° and -120° mechanically apart from phase A, respectively. Fig. 2.1 (b) shows its 3-D exploded view. As the name suggests, each stator has 12 stator poles; whereas the rotor has 10 segments. The stator poles are categorized into two types which are exciting poles (viz. P_{A1}, P_{B1}, P_{C1}, ... P_{A4}, P_{B4}, P_{C4}) and auxiliary poles; adjacent to the exciting poles. The width of exciting poles are wider than the auxiliary poles. The phase windings are only wound on the exciting poles whereas no windings are present on the auxiliary poles. The auxiliary poles only provide the return paths for the flux generated by the exciting poles. The poles of inner and outer stators are in face alignment. The rotor is made of the discrete segments of electrical steel. These segments are magnetically isolated from each other and embedded into a non-magnetic isolator. In the figure, it can be seen that in single-tooth winding topology each stator slot contains the conductors of only one phase, subsequently, this winding topology has a compact structure and expresses more fault-tolerant capability. The winding configuration of a phase (viz. phase A) is shown in Fig. 2.1 (c). Each phase winding has 4 coils which are connected in series. However, they can be connected in parallel also as per the application environment. The polarity of the inner and outer stator coils of a phase is selected in such a way that their fluxes cancel each other near the unaligned rotor position. This characteristics of the machine decreases the unaligned inductance and increases the output torque. In Fig 2.1 (a), the rotor shown is in completely unaligned condition with phase A. The figure also defines the mechanical positions of the motor.

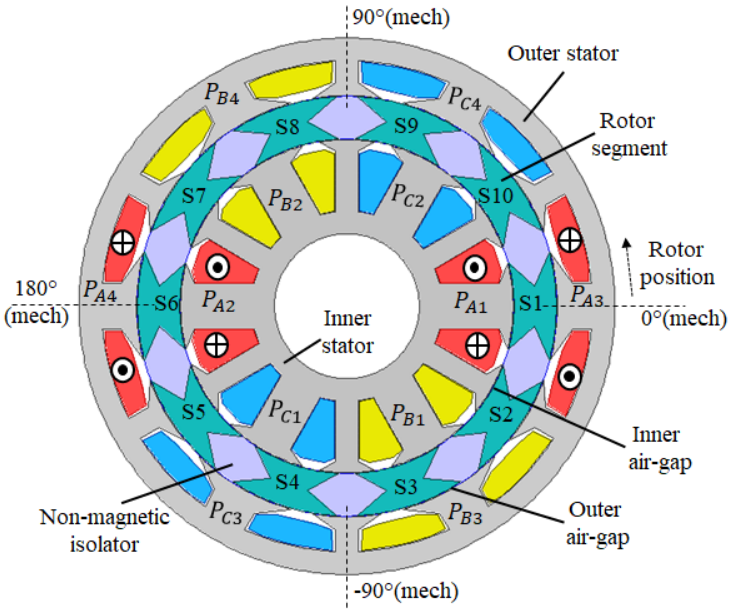

(a)

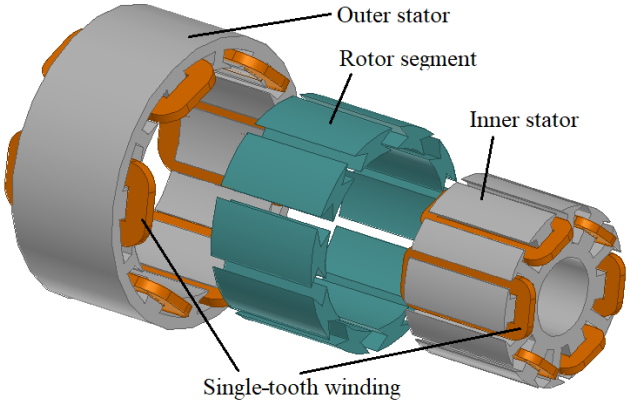

(b)

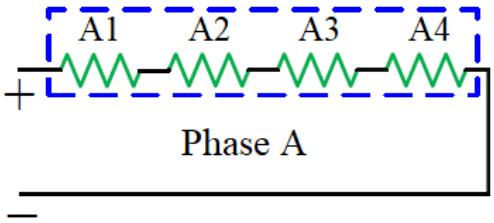

(c)

Figure 2.1: Structure of 3-phase 12/10/12 pole single-tooth winding DSSRM. (a) Cross-sectional view with only phase A windings shown. (b) Exploded view. (c) The phase winding configuration.

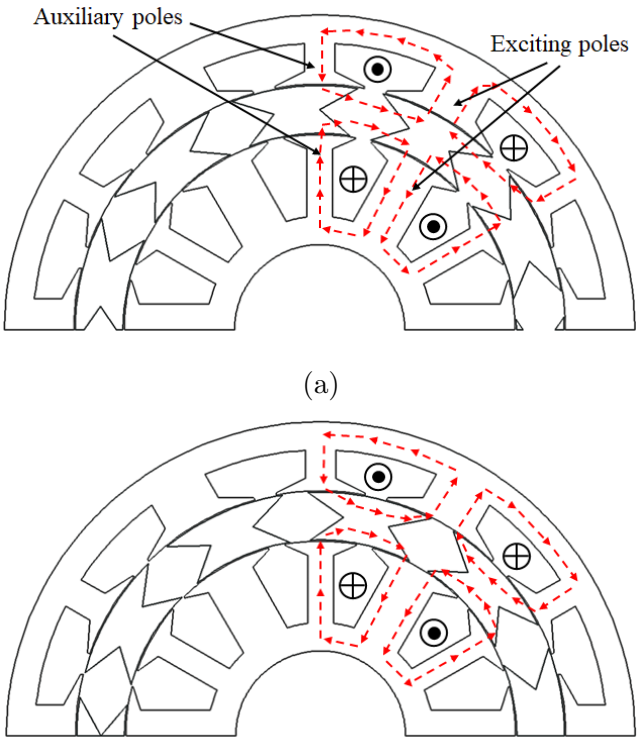

Figure 2.2: Flux distribution pattern and operating principle of DSSRM. (a) Unaligned position. (b) Aligned position.

2.2.2 The operating principle

The operating principle of DSSRM is illustrated in Fig. 2.2, which consider the half section of the motor. The figure illuminates the coils of an excited phase. Fig. 2.2 (a) shows the magnetic flux distribution in the case of unaligned rotor position. The magnetic flux starts from the exciting poles, passes through back iron and the adjacent auxiliary poles, and returns via rotor segments. In this case, the flux has to cross the non-magnetic gaps between the adjacent stator poles, and therefore faces a high magnetic reluctance. To reduce the reluctance, the flux try to pull the nearest rotor segments to fill the gap between the stator poles. Because of the inertia of the rotor, the flux pulls the segments in the direction of rotation. Therefore, the rotor continues the rotation. Fig. 2.2 (b) shows the condition of the aligned position. In this case, the rotor segments bridge the gaps between the adjacent stator poles, and hence the flux has minimum magnetic reluctance.

The above operating principle can be extended for the topology shown in Fig. 2.1.

In this case, for excitation of a phase, 4 different rotor segments come into its magnetic influence (viz. S1, S2, S6 and S7 for phase A), and the rotor will try to magnetically align with this phase. Hence, the rotor can start rotating in the counter-clockwise direction if the phases are energised correctly in the sequence of A-B-C.

2.3 Design concepts of single-tooth winding DSSRM

Although the superiority of the single-tooth winding DSSRM is reported in the literature, the complete design concepts is missing. In this section, the design concepts of the single-tooth winding DSSRM have been represented together with some performance improvements. The SRMs show a non-linear variation in its performance with respect to the variation in its design parameters. Therefore, FEM based simulation study is utilized to yield a more accurate design procedure.

2.3.1 Torque equation

The instantaneous torque developed in an SRM as given by [90]

$$t = \frac{1}{2} i^2 \frac{dl}{d\theta} \tag{2.1}$$

The average torque developed in the motor is as given below

$$T_{avg} = \frac{1}{2} I_p^2 \frac{(L_a - L_u)}{\frac{2\pi}{(N_r\ q)}} \tag{2.2}$$

or

$$T_{avg} = \frac{1}{4\pi}\ I_p^2\ L_a \left(1 - \frac{L_u}{L_a}\right) N_r\ q \tag{2.3}$$

where I_p is the peak value of phase current, L_u and L_a are the unaligned and aligned phase inductances respectively, N_r is the number of rotor segments and q is the total number of phases. The per-phase inductance at the aligned position is given as

$$L_a = \frac{N_{ph}\ B_g\ A_{ol}}{I_p} \tag{2.4}$$

The air-gap flux density B_g near the aligned rotor position is

$$B_g = \frac{N_{ph}\ I_p\ \mu_0}{8 \times m \times l_g} \tag{2.5}$$

Where N_{ph} is the number of turns per phase, l_g is the length of inner and outer air-gaps and m is the multiplicity of the motor.

Substituting Eq. (2.4) in Eq. (2.3); the average torque of the DSSRM is expressed as

$$T_{avg} = \frac{1}{4\pi}\, N_{ph}\, I_p\, B_g\, A_{ol} \left(1 - \frac{L_u}{L_a}\right) N_r\, q \tag{2.6}$$

The overlap area A_{ol} between the stator poles and rotor segments surfaces in aligned position is

$$A_{ol} = (A_{ol\ inner} + A_{ol\ outer})$$

$$A_{ol} = \frac{\pi(D_{ri} + D_{ro}) \times l}{N_r\, q}$$

$$A_{ol} = \frac{2\pi \times D_r \times l}{N_r\, q} \tag{2.7}$$

Substituting Eq. (2.7) in Eq. (2.6) we obtain

$$T_{avg} = \frac{1}{2}\, N_{ph}\, I_p\, B_g \left(1 - \frac{L_u}{L_a}\right) D_r\, l \tag{2.8}$$

$$T_{avg} = \frac{1}{2}\, N_{ph}\, I_p\, B_g\, k\, D_r\, l \tag{2.9}$$

where $D_r = (D_{ri} + D_{ro})/2$ is the average diameter of the rotor, l is the axial length of the motor and $k = (1 - L_u/L_a)$ which can be calculated by FEM based simulation study.

It is seen in Eq. (2.8) that for a given MMF and magnetic loading B_g, the average torque depends on the average diameter of rotor (D_r), axial length (l) of motor and the aligned and unaligned inductances of the phase windings. The value of D_r is dependent on the outer diameter of motor and pole heights the stators. It is clear that a higher output torque is obtained for a higher value of aligned inductance and lower value of unaligned inductance. Therefore, during the design procedure, the proper selection of these parameters is essential to obtain a higher output torque.

2.3.2 Sizing Procedure

Fig. 2.3 shows the half cross-sectional view and a cut view of approximated linear model of DSSRM showing the different parameters of the motor. Fig. 2.3 (a) shows the outer and

inner diameter of the motor (D_o, D_i), the average diameter of rotor (D_r), stator and rotor pole pitch angles (β_{ps}, β_{pr}), stator and rotor slot opening angles (β_{so}, β_{ro}); and exciting pole, auxiliary pole and rotor segment arc angles ($\beta_{exc}, \beta_{aux}, \beta_r$). Fig. 2.3 (b) shows the dimensions of different magnetic parts of stator and rotor. Since the yoke of inner and outer stator bear nearly the same level of magnetic flux density, they have the same width of h_{ys}. As seen in Fig. 2.2, the flux passing through an exciting pole is distributed between two adjacent auxiliary poles. Therefore, the width of the exciting poles (w_{exc}) is twice the width of the auxiliary poles (w_{aux}). Moreover, the flux passing through the yoke of a stator subsequently passes through the auxiliary pole and thereafter half of the height of the rotor segment (h_{pr}). The above field distribution reveals the following conclusions:

$$w_{exc} = 2\ h_{ys} \tag{2.10}$$

$$w_{aux} = h_{ys} \tag{2.11}$$

and

$$h_{pr} \simeq 2\ h_{ys} \tag{2.12}$$

From the above equations, it is observed that the selection of height of stator yoke (h_{ys}) is very important for the design as other parameters are linearly dependent on it. To increase the output torque of the machine, the MMF/slot should be increased ensuring that the maximum flux density in different magnetic parts of the machine is within the maximum permissible limit, B_{max}. This requires to increase the value of h_{ys} with the increase in MMF/slot. To share nearly equal torque and power by inner and outer stators, the MMF/slot for inner and outer stator should be same. This will reduce the radial force on rotor segments also because nearly equal and opposite radial force will be exerted on the rotor segments by the inner and outer stator fluxes. As the inner stator has an enclosed surrounding, poor heat dissipation condition may prevail which can affect its thermal stability and hence, the power density. Therefore, a better cooling arrangement is required to impart thermal stability. The problem of heat dissipation in inner stator can be reduced by decreasing the current density in its windings. This will require higher conductor cross-sectional area and higher slot area for inner stator windings for a given MMF. An increase in the slot area will require the increase in the pole height

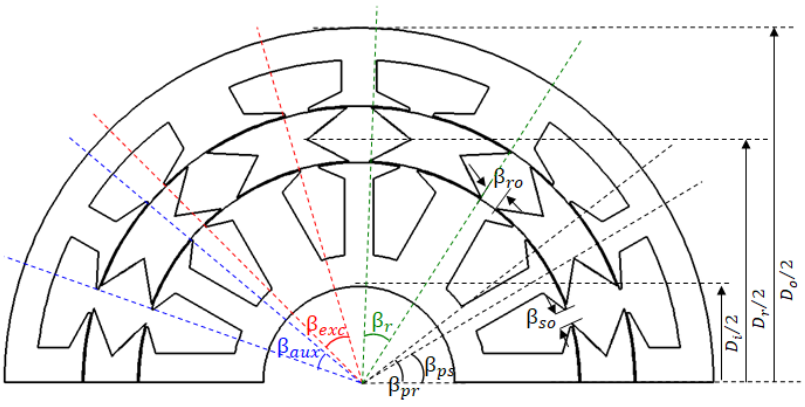

(a)

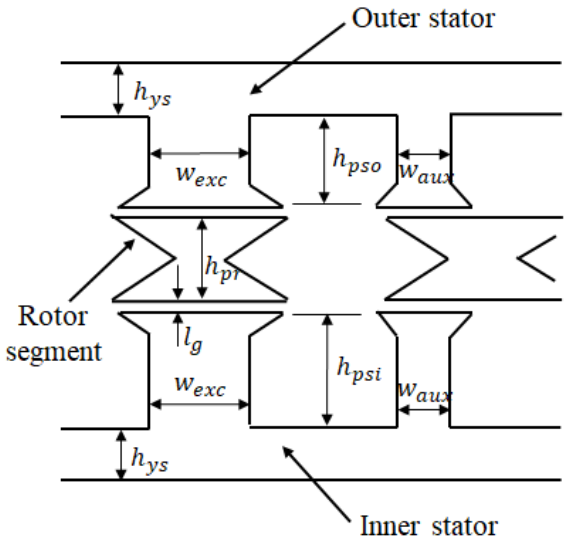

(b)

Figure 2.3: Representation of the design parameters of DSSRM. (a) Half section of 2-D view. (b) Cut view of approximated linear model.

of the inner stator (h_{psi}). Increasing the pole height will further lead to an increase in the motor weight which will reduce the torque/power density of the motor. However, this arrangement will reduce the heat dissipation issue and will improve the thermal stability of the machine. In higher outer diameter machines there is more flexibility to increase the height of inner stator poles. Therefore, in such machines, the lower current density in inner stator windings can be adopted to improve the thermal stability.

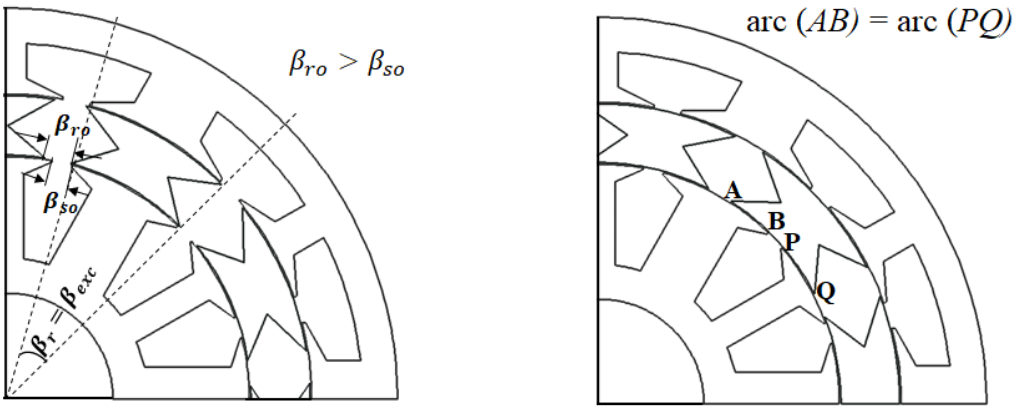

(a) (b)

Figure 2.4: Condition for minimum unaligned and maximum aligned inductances. (a) Minimum unaligned inductance condition. (b) Maximum aligned inductance condition.

2.3.3 Calculation of stator pole and rotor segment arc angles

As seen in Eq. (2.8), the output torque of an SRM is high for the higher value of the difference between aligned and unaligned inductances. For minimum unaligned inductance, the nonmagnetic separation between two adjacent rotor segments (β_{ro}) should not be lesser than the stator slot opening angle (β_{so}). Moreover, the arc angle of rotor segments (β_r) should not be greater than the arc angle of exciting stator poles (β_{ext}). Therefore, the minimum unaligned inductance can be assured by the following two conditions:

$$\beta_{ro} \geq \beta_{so} \tag{2.13}$$

and

$$\beta_r = \beta_{exc} \tag{2.14}$$

The graphical representation for the minimum unaligned inductance condition is given in Fig. 2.4 (a). The condition of maximum aligned inductance can be achieved when the rotor segments overlap area with the exciting and auxiliary poles are equal in aligned rotor position. This condition is graphically represented in Fig. 2.4 (b). In this case, the arc AB and arc PQ have equal span at the aligned condition. This condition can be assured by the following expression:

$$\beta_{exc} - \beta_{aux} = 2 \times (360^\circ/N_r - \beta_{ps}) \tag{2.15}$$

Another geometric relationship between the exciting and auxiliary pole arc angles for a given stator slot opening angle (β_{so}) is:

$$\beta_{exc} + \beta_{aux} = 2 \times (360^{\circ}/N_s - \beta_{so}) \tag{2.16}$$

where β_{exc} and β_{aux} are in degree; N_r and N_s are the number of rotor segments and stator poles respectively. Considering the above constraints the values of β_{exc}, β_{aux} and β_r are as follows:

$$\beta_{exc} = \beta_{pr} - \beta_{so} \tag{2.17}$$

$$\beta_{aux} = 2\beta_{ps} - \beta_{pr} - \beta_{so} \tag{2.18}$$

and

$$\beta_r = \beta_{pr} - \beta_{so} \tag{2.19}$$

The above Eqs. (2.17)–(2.19), give the condition of arc angles for maximum output torque in DSSRM. However, in the case of high-speed motor design, where a high β_{so} is essential, the value of β_r greather than β_{exc} can provide a higher output torque.

2.3.4 Selection of slot/segment combination

To select the number of stator pole and rotor segments for a 3-phase DSSRM, the valid slot/segment combinations are listed in Table 2.1. The combinations with unity multiplicity ($m = 1$) are not considered because of unbalanced magnetic forces are created on the stator surfaces. The combinations of 12/8, 12/10 and 12/14 poles with twice multiplicity ($m = 2$) are considered for the comparison in the view of axial length requirement, unaligned/aligned inductances and total active weight of the machine. Table 2.2 lists the rated operating condition for the comparison of above slot/segment combinations.

Table 2.1: Valid slot/segment combinations for 3-phase single-tooth winding DSSRM.

No. of phases (q)	Multiplicity (m)	Slot/segment combination
3	1	6/4, 6/5, 6/7 etc.
3	2	12/8, 12/10, 12/14 etc.

Table 2.2: Initial design parameters for the rated operation.

Parameter	Value
Number of phases (q)	3
Outer diameter (D_o)	200 mm
Rated power (P_o)	2.5 KW
Rated Speed (N)	600 rpm
Rated torque (T_{avg})	40 N-m

The stator slot opening angle β_{so} is considered in the range of 5°- 6°. The value of β_{so} for 12/8 and 12/10 pole combinations is 6°. However, because of the increase in the number of rotor segments in 12/14 pole combination, β_r reduces considerably. This will reduce the overlapping of rotor segments with exciting and auxiliary poles at the aligned condition and reduces the aligned inductance. Therefore, to increase the aligned inductance, the value of β_{so} is reduced to 5° for this combination. The performance comparison of the different combinations has been done for a 5 A/mm^2 of average phase current with slot fill factor (SFF) of 0.43. To excite the phases, a trapezoidal current wave of 35° (elec.) rising and falling period and 110° (elec.) period of peak value is applied for each motor. The same MMF/slot and same conductor cross-section are considered for inner and outer stator windings. The frequency of current switching per revolution for 12/8, 12/10, and 12/14 pole motor are 24, 30, and 42, respectively.

During the design of DSSRM, the height of stator yoke h_{ys} and pole height of inner and outer stator can be calculated by FEM base simulation study in such a way that maximum flux density in different parts of the machine should be within B_{max}. In this work, B_{max} is considered within 1.8 T and flux density in various magnetic parts of the motor in the aligned position is in the range of 1.4 to 1.7 T. The values of other motor parameters are calculated using Eqs. (2.10)–(2.12) and Eqs. (2.17)–(2.19). The flowchart for the design procedure of DSSRM is shown in Fig. 2.5. The FEM models of the considered slot/segments combinations are developed using above design procedure. The outer and inner diameters are considered same for each motor which are 200 mm and 54 mm, respectively. The simulated result data for the rated condition are listed in Table 2.3.

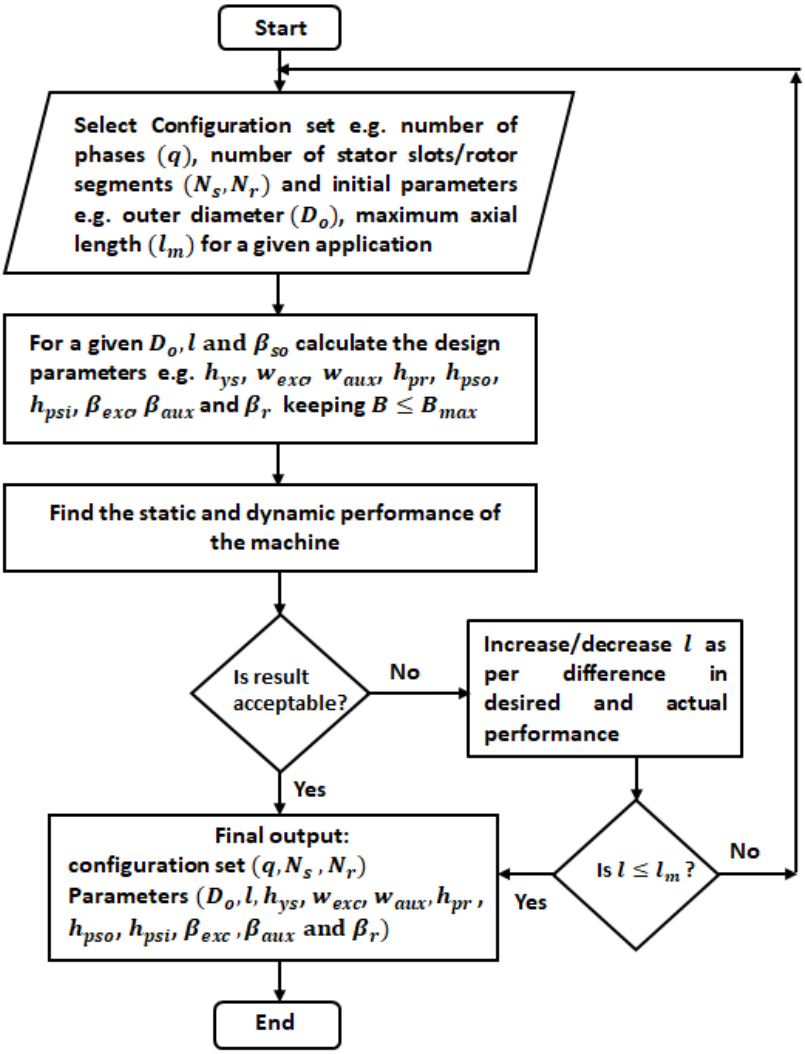

Figure 2.5: Flowchart for the design procedure of DSSRM.

Table 2.3: Comparison between different slot/segment combinations of DSSRM.

Parameter	12/8 pole	12/10 pole	12/14 pole
Torque T_{avg} in N-m	40.7	40.3	40.5
Axial length (l) in mm	106	85	94
Unaligned inductance(L_u) in mH	4.39	3.39	4.85
Aligned inductance (L_a) in mH	25.80	21.10	17.39
Iron weight in kg	14.36	11.61	12.54
Copper weight in kg	3.23	2.76	3.10
Total active weight in kg	17.59 (122%)	14.37 (100%)	15.64 (109%)

It is observed that the axial length required for the rated torque generation in 12/10 pole combination is 85 mm which is nearly 8/10 times of the 12/8 pole combination. This is because of the higher number of strokes per revolution (i.e. 10/8 times) in 12/10 pole motor as compared to 12/8 pole motor, which increases the torque density in it. This is the same case as in conventional SRM where the output torque increases with the increase in the number of rotor poles. Furthermore, because of the higher axial length, the value of L_u, L_a and total active weight is high in 12/8 pole machine as compared to 12/10 pole combination. The further increase in the number of rotor segments as in 12/14 pole motor, the condition as given in Eq. (2.13) is violated, subsequently the assurance of minimum inductance and maximum reluctance at unaligned position diminishes. The value of L_u increases and torque density reduces. Therefore, the benefit of a higher number of strokes per revolution becomes ineffective in this case. The axial length required for rated torque generation increases to 94 mm in this case, subsequently, the total active weight of the machine also increases. Therefore, for the rated operation, 12/10 pole combination has better performance over other variants and is considered for further analysis in this work.

2.3.5 Influence of winding polarities

In SRMs, two phases are excited at the same time during the commutation period to increase the output torque and to reduce torque ripple. However, the excitation patterns

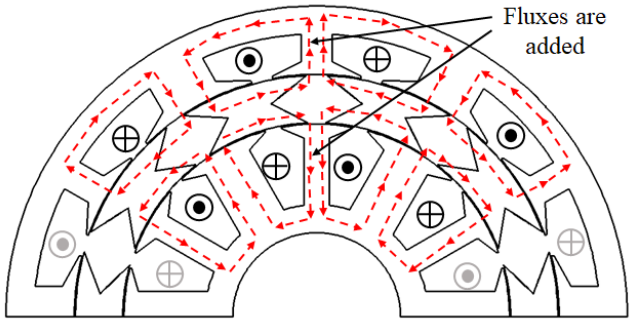

(a)

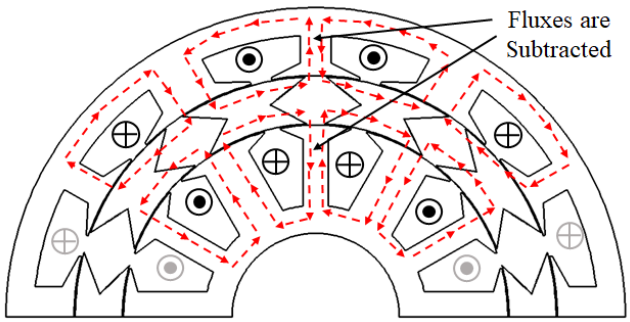

(b)

Figure 2.6: Flux dissemination for the simultaneous excitation of two phases. (a) Aiding flux winding polarity. (b) Subtracting flux winding polarity.

of two consecutive phase windings have different influence on its performance. Fig. 2.6 shows the possible winding polarities for the DSSRM with their flux patterns. Fig. 2.6 (a) shows the aiding flux winding polarity in which the fluxes of two adjacent phases are in the same direction in the auxiliary pole and it carries the summation of the fluxes. This winding pattern has no flux reversal in the auxiliary poles, however, there may be saturation condition in the auxiliary poles because of the summation of the fluxes. Fig. 2.6 (b) illustrates the subtracting flux winding polarity in which the fluxes of two adjacent phases are in opposite direction in the auxiliary pole and it carries the difference of the fluxes. This winding pattern will reduce the saturation condition in the auxiliary poles, but there is flux reversal when motor commutates from one phase to the next phase. To select the suitable winding polarity for the rated operation, further analysis has been done in this work.

Fig. 2.7 shows the variation of the magnetic flux density in the different parts of the 12/10 pole motor at rated speed. The mid-point or center point of the respective

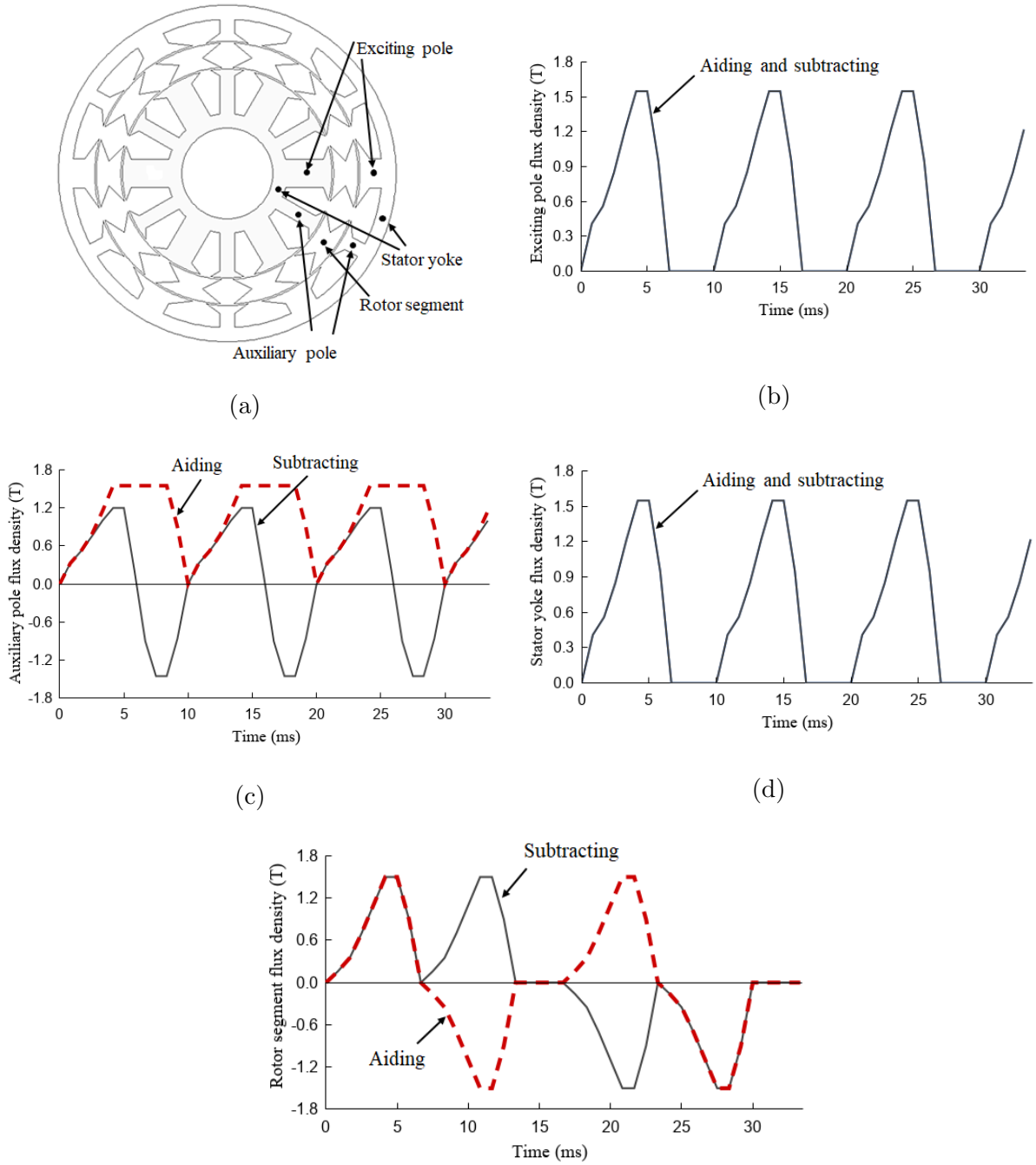

Figure 2.7: Flux density variation in different parts of DSSRM for aiding and subtracting flux winding polarities. (a) Geometry points for flux density calculation. (b) Exciting pole. (c) Auxiliary pole. (d) Stator yoke. (e) Rotor segment.

parts are considered to measure the flux density which is shown in Fig. 2.7 (a). It can be seen that the flux density waveforms are periodic and non-sinusoidal in the different parts of the motor. The frequency of the flux waveforms in the exciting pole, auxiliary pole and stator yoke is 100 Hz, while in rotor segments it is 60 Hz and 30 Hz for aiding and subtracting flux winding polarities, respectively. Therefore, determining the sinusoidal components of these loss-causing flux density waveforms is essential [91]. Table 2.4 deals with this data. It can be observed in Fig. 2.7 (b) and Fig. 2.7 (d) that the flux reversal in the exciting pole and stator yoke of the machine is absent. From the data given in the table, it is clear that the machine with aiding flux winding polarity has a higher dc component in the auxiliary pole. This will increase the saturation condition and output torque will reduce. However, in the case of subtracting flux winding polarity, flux reversal exists in auxiliary pole as shown in Fig. 2.7 (c). From the table data, it is clear that in this case the fundamental frequency component is high, which eventually increases the core losses. The performances of the DSSRMs with aiding and subtracting flux winding polarities for the rated output torque are simulated and the results are listed in Table 2.5. It is observed that the aiding flux winding polarity has slightly lower core losses, however, for the rated output torque, it requires slightly higher axial length and active weight as compared to the subtracting flux winding polarity. For the considered rated operating condition, subtracting flux winding polarity shows slightly better performance and therefore, it is selected for further analysis in this work.

2.4 Simulation results

Table 2.2 and Table 2.6 gives the details of the design specifications of the 3-phase 12/10 pole DSSRM. The 2-D FEM model is established in ANSYS/MAXWELL software to obtain the electromagnetic performance of the DSSRM. The basic steps followed for the analysis are modelling, assigning material properties, assigning boundaries, meshing, providing excitation and analysis set-up and finally, the response is simulated. The core material selected for stator and rotor is 'steel-1008' which is imported from the software library. To calculate the core losses 0.4 mm thickness of laminations is considered. The zero vector potential boundary is considered just above the outer surface of the model so that the flux does not move outside of this surface.

Table 2.4: Magnitude of the different harmonics of flux densities in different part of DSSRM.

Flux density (T)								
Harm.	Exc. pole		Aux. pole		Stator yoke		Rotor segment	
order	W1	W2	W1	W2	W1	W2	W1	W2
DC	0.59	0.59	1.08	0.05	0.59	0.59	0	0
1	0.78	0.78	0.70	1.24	0.78	0.78	1.05	0.98
2	0.24	0.24	0.24	0.46	0.24	0.24	0.45	0
3	0.15	0.15	0.16	0.03	0.15	0.15	0.25	0.29
4	0.07	0.07	0.11	0.08	0.07	0.07	0.22	0
5	0.03	0.03	0.05	0.01	0.03	0.03	0	0.59

W1- aiding flux winding polarity, W2- subtracting flux winding polarity

Table 2.5: Comparison between aiding and subtracting flux winding polarities.

Parameter	Aiding flux	Subtracting flux
Torque T_{avg} in N-m	40.0	40.1
Axial length (l) in mm	87.5	86
Core loss in W	50	53
Iron weight in kg	11.96	11.75
Copper weight in kg	2.81	2.78
Total active weight in kg	14.77	14.53

Table 2.6: 12/10 pole DSSRM design specifications.

Parameter	Value
Outer and inner diameters (D_o, D_i)	200 mm, 54 mm
Average diameter of rotor (D_r)	140.5 mm
Axial length (l)	86 mm
Stator yoke iron width (h_{ys})	8.5 mm
Stator slot opening angle (β_{so})	6°
Arc angle of exciting and auxiliary poles (β_{exc}, β_{aux})	30°, 18°
Rotor segments arc angle and separation angle (β_r, β_{ro})	30°, 6°
Inner and outer air-gap length (l_g)	0.4 mm
Number of conductors per slot	54
Phase resistance	0.471 Ω
Peak phase current	26 A

2.4.1 Static analysis

Figs. 2.8 (a) and 2.8 (b) show the magnetic flux density vectors for the unaligned and aligned rotor positions, respectively with the excitation of the phase winding with rated 26 A current. It is seen that in the unaligned position the flux density vectors are very weak because of the high reluctance; and will try to pull the rotor towards the aligned position. The figures also illustrate that this topology follows the low flux path pattern and increases the electrical utilisation of the machine. Fig. 2.9 represents the magnetic flux density distribution in the different active parts of the motor with the rated excitation of a phase winding. The flux density in stator and rotor are in the range of 1.5 to 1.8 T in the aligned position. Fig. 2.10 shows the static inductance and torque profiles for the positive torque generating region. The phase windings have very low unaligned inductance because of the cancellation of inner and outer stator fluxes near the unaligned position.

2.4.2 Steady-state analysis

The response of the 12/10 DSSRM is simulated for the rated speed of 600 rpm. To obtain the steady-state waveforms, a conventional 3-phase asymmetric half-bridge converter is

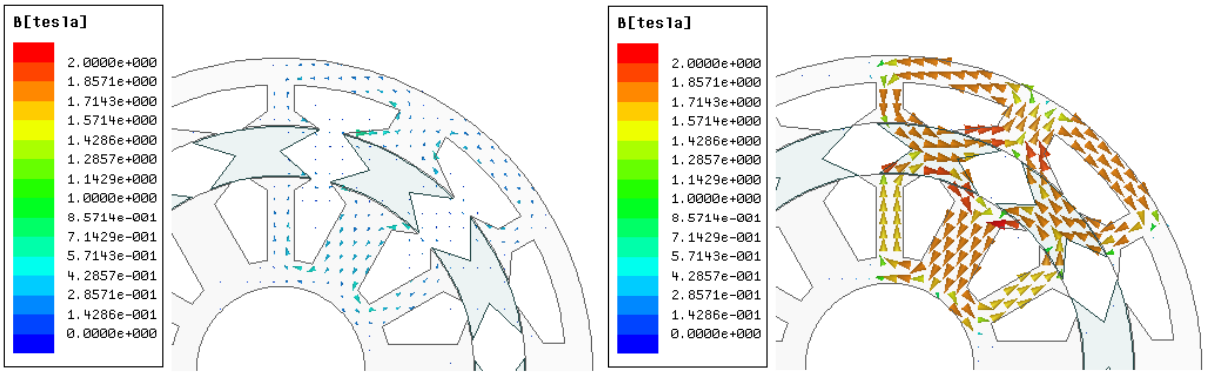

(a) (b)

Figure 2.8: Magnetic flux density vectors for rated 26 A excitation of a phase. (a) Unaligned position. (b) Aligned position.

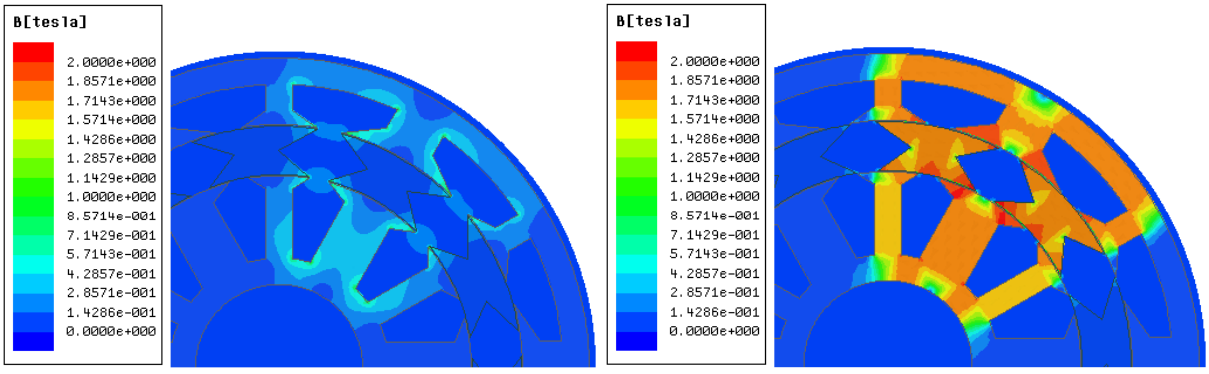

(a) (b)

Figure 2.9: Magnetic flux density distribution for rated 26 A excitation of a phase. (a) Unaligned position. (b) Aligned position.

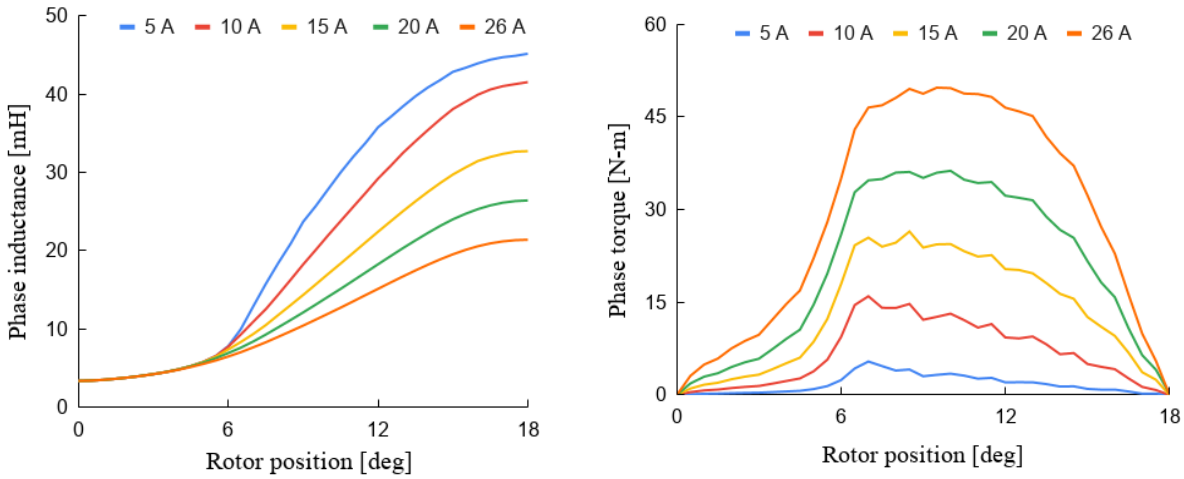

(a) (b)

Figure 2.10: Static inductance and torque profiles. (a) Static inductance. (b) Static torque.

used, which utilises two switches per phase and provides maximum control flexibility [90]. The phase turn-on and turn-off angles considered are 0° and 14.5° (mech.), respectively. To maintain the phase currents, hysteresis current control is used with the hysteresis band of ± 0.4 A and the reference current of 26 A. The phase current overlap technique is used to increase the output torque and to reduce the torque ripple [92]. The calculation of the torque ripple and the efficiency of the motor are carried out by the Eqs. (2.20) and (2.21), respectively.

$$T_{ripple} = (T_{max} - T_{min})/T_{avg} \tag{2.20}$$

$$\eta = P/(P + P_{Fe} + P_{Cu}) \tag{2.21}$$

where T_{max}, T_{min} and T_{avg} are the maximum, minimum and average value of the output torque respectively. η, P_{Fe} and P_{Cu} are the efficiency, iron loss and copper loss respectively, and P is the total output power without mechanical loss.

Fig. 2.11 shows the variation of the phase currents and torque with rotor position in steady-state condition. The machine produces the rated output torque of 40.1 N-m. The peak-to-peak torque ripple and %torque ripple are 31.5 N-m and 78.5%, respectively. This shows the presence of high torque ripple in the motor. The phase resistance and per phase rms current are 0.471 Ω and 16 A, respectively. The copper loss and core loss are 362 W and 53 W, respectively. The rated efficiency is 85.8%. Table 2.7 lists the

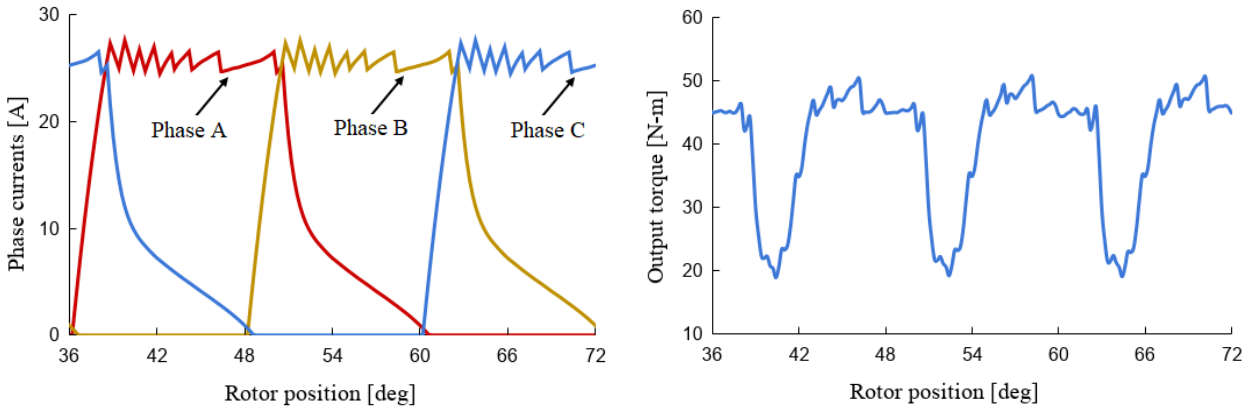

(a) (b)

Figure 2.11: Phase currents and torque variation with rotor position at steady-state condition. (a) Phase currents. (b) Output torque.

performance data for DSSRM at the rated operating condition.

Table 2.7: Performance data of 12/10 pole DSSRM at rated operating condition.

Parameter	Value
Rated speed (N)	600 rpm
Average torque (T_{avg})	40.1 N-m
Peak-to-peak torque ripple (T_{pk2pk})	31.5 N-m
Torque ripple (T_{ripple})	78.5%
Unaligned inductance (L_u)	3.53 mH
Aligned inductance (L_a)	21.85 mH
Core loss (P_{Fe})	53 W
Copper loss (P_{Cu})	362 W
Rated efficiency (η)	85.8%

An FEM model of 24/20 pole DSSRM with multiplicity $m = 4$ is also developed and the steady-state response is simulated to check its torque pulsation behaviour. Table 2.8 list the design data for this motor. The rated power of the motor is 5 kW with the rated speed of 600 rpm. Table 2.9 shows the performance data for this motor. The torque ripple for the rated condition is 108.4%. This investigation shows the presence of high torque ripple in this motor also.

Table 2.8: 24/20 pole DSSRM design data.

Parameter	Value
Outer diameters (D_o)	292 mm
Average diameter of rotor (D_r)	229.5 mm
Axial length (l)	86 mm
Stator yoke iron width (h_{ys})	8.4 mm
Stator slot opening angle (β_{so})	3.5°
Arc angle of exciting and auxiliary poles (β_{exc}, β_{aux})	14.5°, 8.5°
Rotor segments arc angle and separation angle (β_r, β_{ro})	14.5°, 3.5°
Inner and outer air-gap length (l_g)	0.4 mm
Number of conductors per slot	42
Peak phase current	23 A

Table 2.9: Performance data for 24/20 pole DSSRM.

Parameter	Value
Rated speed (N)	600 rpm
Output torque (T_{avg})	81.3 N-m
Torque ripple (T_{ripple})	108.4%
Core loss (P_{Fe})	297 W
Copper loss (P_{Cu})	394 W
Rated efficiency (η)	88.0%

2.5 Comparison with conventional SRM

The performance of the 12/10 DSSRM is compared with the conventional 12/8 pole SRM. The comparison is made with the constraints that output torque, outer diameter and slot fill factor are considered same in both cases. The performances are simulated for the rated speed of 600 rpm. The comparison data is given in Table 2.10. It is seen that the active axial length required in DSSRM is considerably low as compared to the SRM for the rated operation. Therefore, total active weight is also low in DSSRM for the required operation. The volumetric torque density of DSSRM is 61% more than SRM. These observations conclude that DSSRM better utilizes the core and machine volumes and reduces the sparsity of the motor.

Table 2.10: Comparison with conventional 12/8 pole SRM.

Parameter	SRM	DSSRM
Torque (T_{avg}) in N-m	40.0	40.1
Outer diameter (D_o) in mm	200	200
Axial length (l) in mm	138	86
Iron weight in kg	19.44	11.75
Copper weight in kg	3.20	2.78
Total active weight in kg	22.64	14.53
Core loss (P_{Fe}) in W	64	53
Copper loss (P_{Cu}) in W	419	362
Efficiency (η) in %	83.9	85.8
Torque density in N-m/L	9.25 (100%)	14.87 (161%)

2.6 Conclusions

In this chapter, the design concepts of single-tooth winding DSSRM are discussed. The torque equation is derived for this configuration. The equations for the arc angles of the stator and rotor poles for low unaligned and high aligned inductances are also derived to obtain the high output torque. Based on these equations, the selection procedure for the number of stator slots/rotor segments is discussed. It is observed that for 3-

phase DSSRM, 12/10 pole combination has better torque density over 12/8 and 12/14 pole combinations. In 12/10 pole combination, higher torque is achieved as compared to 12/8 pole combination because of the higher number of strokes per revolution; however, in 12/14 pole combination, the benefit of the higher number of strokes per revolution becomes ineffective because of the significant increase in unaligned inductance. Furthermore, the influence of winding polarities on the performance of DSSRM is investigated. It is observed that unlike subtracting flux winding polarity, aiding flux winding polarity has no flux reversal in auxiliary poles; therefore, it has lower core loss. However, it has lower torque density as compared to subtracting flux winding polarity because of higher saturation in auxiliary poles. For the rated operating condition the subtracting flux winding polarity has overall better performance over the other one and therefore considered for further analysis in this work. The steady-state performance of this motor is simulated through the FEM. The output response shows the presence of high torque ripple in it, and devulges the need of further improvement in its torque pulsation behaviour.

The next chapter discusses some design modification techniques in DSSRM to mitigate the torque ripple in it.